



Experimental and numerical analysis of flow behavior and particle distribution in A356/SiCp composite casting



Feifan Chen^{a,*}, Haidong Zhao^a, Gang Zhu^a, Paixian Fu^b, Lijun Xia^b

^a National Engineering Research Center of Near-net-shape Forming for Metallic Materials, South China University of Technology, Guangzhou 510640, China

^b Shenyang National Laboratory for Materials Science, Institute of Metal Research, Chinese Academy of Sciences, Shenyang 110016, China

ARTICLE INFO

Article history:

Received 12 August 2014

Received in revised form 28 February 2015

Accepted 4 April 2015

Available online 11 April 2015

Keywords:

A356/SiCp composite

Real-time X-ray radiography

Flow behavior

Particle distribution

ABSTRACT

Flow behavior and particle distribution in an inverted U-shape A356/SiCp composite casting produced by conventional investment casting were investigated experimentally and numerically. The mold filling process was directly observed by real-time X-ray radiography and the SiCp contents in casting different parts were quantitatively measured and analyzed. Based on the Euler and Lagrangian methods, the flow behavior of composite slurry and the particle distribution were simulated. During mold filling process, eddy flow occurred at gravity part and back flow formed at horizontal part after the gravity part had filled. The predicted results of particle trajectories showed that the flow characteristic of particles were turbulence, laminar, and large eddy flow at anti-gravity, horizontal, and gravity part, respectively. For the particle distribution, the measured and predicted results showed that more particles concentrate in the central section, while fewer particles were present near the surface section along the thickness. Moreover, the particle fractions generally decreased with the increasing distance to the ingate. The simulate results were reasonably suited with experimental data.

© 2015 Elsevier Inc. All rights reserved.

1. Introduction

Casting process is widely used in particle-reinforced aluminum matrix composites (PR-AMCs) in terms of ease to product components with complex shapes and lower cost [1,2]. Among the casting processes, investment casting combined with stir casting method is a particularly attractive one [3]. The stir casting method is a traditional and simple way to obtain PR-AMCs slurry. The investment casting method is a precision casting process, capable of producing high accurate, excellent surface finish and complex shaped casting. In the investment casting process, a wax patterns is produced, followed by shell building and shell de-waxing, then the liquid metal is poured into the shell mold [4]. Due to the poor machinability and workability of components in PR-AMCs, the investment casting method can be a valuable option to produce near-net-shape composite products [3,5].

For PR-AMCs fabricated by casting process, the particle distribution has significant effect on the casting properties, especially particle segregation [6,7]. The particle segregation may take place during three stages in casting process: stirring, mold filling, and

solidification [8]. In previous studies have been developed various investigations related to the particle segregation during stirring and solidification stages but very little about mold filling stage [9–12]. According to multi-phase fluid dynamics theory [13], flow behavior of fluid during mold filling should have important effect on the particle distribution. As always, researchers expect to observe the flow behavior of molten metal directly during mold filling process. Because of high temperature of melt and opacity of mold, this goal did not come true until the emergence of the real-time X-ray radiography technique [14,15]. Some researchers have observed the alloy filling process directly by using this technique [16–19]. However, observation of mold filling of composite casting has not been reported yet. To implement the composite casting successfully in the industry, it is thus important to understand the flow behavior of the slurries and the particle distribution.

In the present study, the A356/SiCp composite casting produced by conventional investment casting was conducted. The mold filling processes were directly observed by real-time X-ray radiography and the SiCp contents at different regions were quantitatively measured and analyzed. The flow behavior of A356/SiCp composite during the mold filling and particle distribution were simulated. In addition, the simulation results were compared and validated with the experimental data.

* Corresponding author. Tel./fax: +86 20 8711 2111.

E-mail address: chenff01@126.com (F. Chen).

Nomenclature

∇	Hamiltonian operator (dimensionless)
c_c	composite heat capacity (J/°C)
c_f	fluid heat capacity (J/°C)
c_p	particle heat capacity (J/°C)
C_D	drag coefficient (dimensionless)
d_p	particle diameter (m)
\vec{F}_f	fluid mass force (N)
\vec{F}_p	particle mass force (N)
P	pressure (Pa)
Re	particle Reynolds number (dimensionless)
S_T	source term (J)
t	time (s)
T	temperature (°C)
\bar{u}_c	composite mean velocity (m/s)
\bar{u}_f	fluid velocity (m/s)
\bar{u}_p	particle velocity (m/s)

Greek symbols

α_f	fluid volume fraction (dimensionless)
α_p	particle volume fraction (dimensionless)
λ_c	composite thermal conductivity (W m ⁻¹ K ⁻¹)
λ_f	fluid thermal conductivity (W m ⁻¹ K ⁻¹)
λ_p	particle thermal conductivity (W m ⁻¹ K ⁻¹)
ρ_c	composite density (kg/m ³)
ρ_f	fluid density (kg/m ³)
ρ_p	particle density (kg/m ³)
μ	viscosity (Pa s)

Subscripts

c	composite
f	fluid
p	particle

2. Experimental works

2.1. Materials and equipment

Aluminum A356 (Al–7 wt.% Si–0.3 wt.% Mg) was selected as the matrix alloy and SiC particles with average size of approximately 50 μm were used as the reinforcements. The composite slurry was prepared by stir casting technology. The well-known problem faced by this technology consisting in poor wetting between ceramic particles and molten aluminum can be overcome by using the double stirring method [4]. This method involves the addition of particle reinforcement into semi-solid metal (SSM) and particle homogenization process at liquid condition.

An inverted U-shape casting (see Fig. 1) including anti-gravity (R1–R3), horizontal (R3–R6) and gravity parts (R6–R8) was designed, and ceramic shell was used as the mold. Real-time X-ray radiography equipment (as shown in Fig. 2) manufactured by GE Inspection was used to directly observe the actual flow behavior of the composite slurry during mold filling process. The equipment mainly consists of an X-ray source/detector pair, an image intensifier, a high speed video camera, a rotating motor, a control

system and a monitor. The voltage and current of the X-ray were 225 kV and 16 mA, respectively. X-ray radiographic images were recorded by using the high speed video camera (further details available online at <http://www.ge-mcs.com/en/inspection-technologies.html>).

2.2. Ceramic shell preparations

A 3D model of casting was designed, and then a metal die was manufactured. The melted wax was poured into the metal die to produce disposable wax pattern. Then the wax pattern was dipped into primary ceramic slurry followed by immediate stuccoing with fine refractory sand and to dry in a controlled environment. After the primary coats had been applied, the next step as well as the above, but the sand having larger particle sizes. The dipping, stuccoing, and drying process were repeated until the ceramic shell was thick enough. When the ceramic shell was completed, and then was subjected to 20 h of extended drying to make them as strong as possible. Finally, the wax inside the dried ceramic shell mold was removed by autoclave de-waxing procedure followed by burning at 1000 °C for 2 h in a resistance furnace. An example of ceramic shell is shown in Fig. 3.

2.3. Melt and casting procedures

To prepare composite slurry, the weighted SiC particles with 10% of nominal reinforced volume fractions of the objective composites were washed in chemical reagent ethanol with an

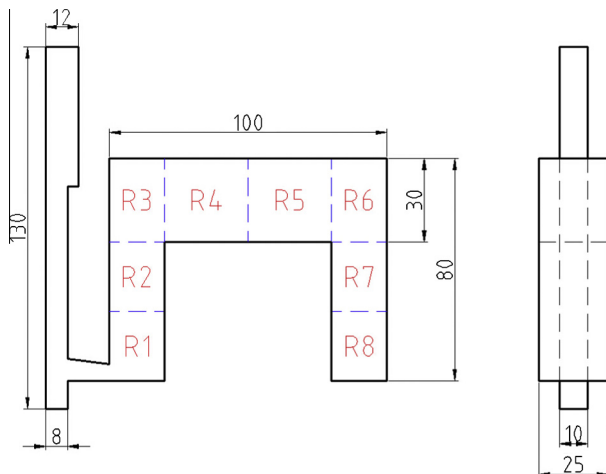


Fig. 1. Schematic of the inverted U-shape casting.

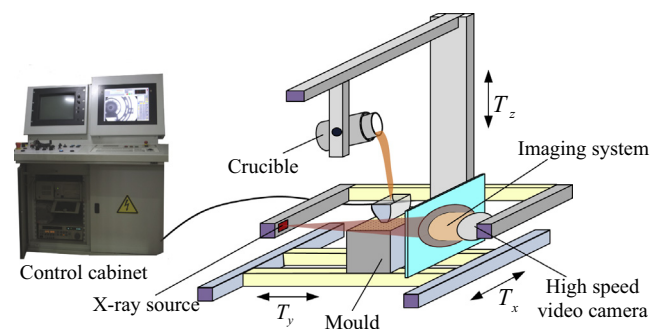


Fig. 2. X-ray system for flow observation.



Fig. 3. Ceramic shell (including pouring basin) after burning step.

ultrasonic cleaner, and then were heated at 70 °C for 12 h to remove moisture. The particles were artificially oxidized in air at 900 °C for 4 h before being added into the molten alloys. The pre-treatment could improve the wettability between the reinforcement particles with aluminum molten matrix due to formed SiO₂ layer on the particle surfaces [20,21]. Moreover, the pre-oxidized SiC particles can minimize the undesired interfacial reaction [22]: $3\text{SiC} + 4\text{Al} \rightarrow \text{Al}_4\text{C}_3 + 3\text{Si}$, giving the fragile carbide Al₄C₃, which is particularly harmful. The weighted quantity of A356 alloys were melted to 720 °C in crucible. After melting, the A356 melt was degassed and fluxed using hexachloroethane, and then cooled to 605 °C in a semi-solid state. The oxidized SiC particles were regularly added to the semi-solid slurry by using a graphite impeller at a speed of 300 rpm to create a vortex. These oxidized SiC particles were pre-heated at 300 °C to evaporate the moisture and to prevent chilling of the alloy during particle addition [23]. Then the composite slurry was reheated to 720 °C and stir again for 30 min at a speed of 150 rpm. The depth of the immersed stirrer was approximately 20% heights of the molten metal from the crucible bottom. According to the works [9–11], these stirring parameters can produce a uniform distribution of SiC in Al/SiCp composite slurry. In the whole stirring stage, argon gas was used to protect the melt against oxidation and avoid the entrapment of gases. After the second stirring, the slag on the surface of composite slurry was removed.

Before pouring process, the ceramic shell was pre-heated at 550 °C and the X-ray radiographic equipment was adjusted. After the composite slurry, ceramic shell and X-ray equipment were all prepared, the A356–10% SiCp composite slurry obtained by stir casting was gravity poured into the ceramic shell. The pouring temperature was 720 °C. During the mold filling process, the X-ray source beam passed through the ceramic shell, and the detector received the X-ray, then the high speed video camera captured the X-ray radiographic image after it was enhanced by image intensifiers.

After cooling, the ceramic shell was removed and then the casting was divided into two parts along the thickness direction of the center by wire-cutting. Samples for assessment of the SiC particle distribution were directly obtained from the casting at central and surface section along the thickness direction, respectively. The microstructure of the samples was observed by Leica optical microscopes. Furthermore, to be able to analyze the SiC particle distribution quantitatively, both central and surface section were

divided into eight regions as shown in Fig. 1. At each region, at least 40 metallurgical photos (at 100× magnification) were obtained by optical microscope. Then the total area of SiC particles out of the total micrograph area was quantified by means of Image-Pro Plus software to indicate the particle volume fraction.

3. Employed numerical procedure

In this section, the two-phase flow models using for simulating the mold filling process will be formulated. Two phases flowed during this process, including particle and molten matrix alloy. The molten metal and the particle phase in the mold are treated as incompressible viscous flow. In the simulation of the mold filling, the Euler approach is applied to solve the molten alloy flow by solving continuity and momentum equations as follows [24]:

$$\text{Continuity equation} \quad \frac{\partial}{\partial t}(\alpha_f \rho_f) + \nabla \cdot (\alpha_f \rho_f \vec{u}_f) = 0 \quad (1)$$

$$\text{Momentum equation} \quad \frac{\partial}{\partial t}(\alpha_f \rho_f \vec{u}_f) + \nabla \cdot (\alpha_f \rho_f \vec{u}_f \vec{u}_f) = -\alpha_f \nabla P + \alpha_f \mu \nabla^2 \vec{u}_f + \vec{F}_f \quad (2)$$

where α_f , ρ_f and \vec{u}_f are the fluid volume fraction, density and velocity, respectively, μ is the dynamic viscosity, t is the time, P is the static pressure, and \vec{F}_f is the fluid mass force.

The fluid volume fraction, α_f , is defined as:

$$\alpha_f = 1 - \alpha_p \quad (3)$$

where α_p is the particle volume fraction.

The particle motion was predicted by using the Lagrangian approach. The trajectory of particle can be determined by solving the equation of particle motion which is governed by:

$$\frac{d\vec{u}_p}{dt} = -\frac{1}{\rho_p} \nabla P + \frac{3}{4d_p} C_D (\vec{u}_f - \vec{u}_p) |\vec{u}_f - \vec{u}_p| \frac{\rho_f}{\rho_p} + \vec{F}_p \quad (4)$$

where \vec{u}_p and ρ_p are the particle velocity and density, respectively, \vec{F}_p is the particle mass force, C_D is the drag coefficient. For spherical particles this drag coefficient is given by the empirical relation [25]:

$$C_D = \begin{cases} \frac{24}{Re} (1 + 0.15Re^{0.678}), & Re < 1000 \\ 0.44, & Re \geq 1000 \end{cases} \quad (5)$$

where Re is the particle Reynolds number, which is calculated as:

$$Re = \frac{d_p \rho_p |\vec{u}_f - \vec{u}_p|}{\mu} \quad (6)$$

During the mold filling process, the temperature changes in the composite slurry are governed by energy equation:

$$\frac{\partial T}{\partial t} + \vec{u}_c \cdot \nabla T = \frac{\lambda_c}{\rho_c c_c} \nabla^2 T + \frac{S_T}{\rho_c} \quad (7)$$

where T , \vec{u}_c , λ_c , ρ_c , and c_c are the temperature, mean velocity, thermal conductivity, density and heat capacity of the composite slurry, respectively, S_T is the source term.

The composite consists of the matrix metal and the ceramic particles which differ in thermal conductivity, specific heat and density. Moreover, some variables are dependent on the ceramic particle fraction. The mean values of the above parameters are calculated by the following equations [26]:

$$\rho_c = \alpha_f \rho_f + \alpha_p \rho_p \quad (8)$$

$$c_c = \frac{\alpha_f c_f \rho_f + \alpha_p c_p \rho_p}{\rho_c} \quad (9)$$

Table 1
Parameters used in the simulation.

Property	Value
Density of A356 (liquid) [27]	$2.392 \times 10^3 \text{ kg/m}^3$
Density of A356 (solid) [27]	$2.68 \times 10^3 \text{ kg/m}^3$
Density of SiC particle [28]	$3.2 \times 10^3 \text{ kg/m}^3$
SiC particle diameter	50 μm
Pouring temperature	720 $^\circ\text{C}$
Latent heat of fusion [28]	$3.89 \times 10^5 \text{ J/kg}$
Specific heat of A356 [28]	$1.08 \times 10^3 \text{ J/kg} \cdot ^\circ\text{C}$
Specific heat of SiC particle [28]	$1.3 \times 10^3 \text{ J/kg} \cdot ^\circ\text{C}$
Thermal conductive of A356 (liquid) [27]	67.9 $\text{W/m} \cdot ^\circ\text{C}$
Thermal conductive of A356 (solid) [27]	145 $\text{W/m} \cdot ^\circ\text{C}$
Thermal conductive of SiC particle [5]	125.6 $\text{W/m} \cdot ^\circ\text{C}$
Viscosity [23]	$4 \times 10^{-3} \text{ Pa s}$

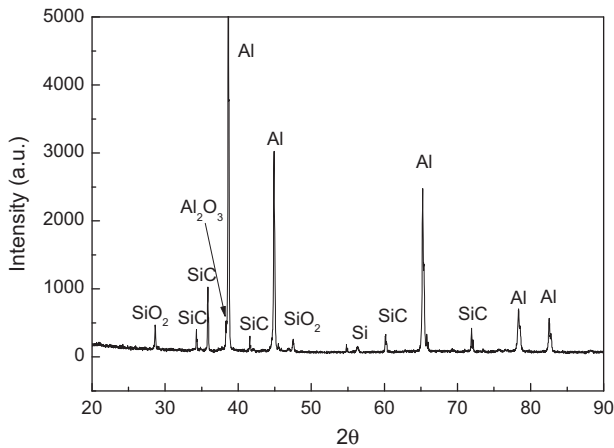


Fig. 4. X-ray diffraction of the composite casting.

$$\lambda_c = \lambda_f \left[\frac{2\lambda_f + \lambda_p - 2\alpha_p(\lambda_f - \lambda_p)}{2\lambda_f + \lambda_p + \alpha_p(\lambda_f - \lambda_p)} \right] \quad (10)$$

where c_p is the particle heat capacity, c_f is the fluid heat capacity, λ_p is the particle thermal conductivity, λ_f is the fluid thermal conductivity.

The equations characterizing the mold filling and particle motion are solved with the scheme embodied in the Flow-3D code. Flow-3D is a general purpose computational fluid dynamics (CFD) package which uses the volume of fluid (VOF) technique to model free surface flows.

In the simulation, pressure and velocity boundary were used for the fluid and particle inlet condition, respectively. Since the falling stream in the experiment was 0.1 m higher than the sprue entrance, the boundary pressure of $2.3 \times 10^3 \text{ Pa}$ was applied. Particles were randomly distributed at the inlet with zero initial velocity. In addition, no-slip wall boundary condition was imposed in the simulation. Parameters used for simulation are tabulated in Table 1.

4. Results and discussions

4.1. Flow behavior

Fig. 4 shows the X-ray diffraction of the composite casting after liquid stirring. It is seen that the formation of Al_2O_3 was detected. The reaction may take place between the particle layer (the SiO_2 layer on the particle surfaces) and Al fluid. And almost all particles

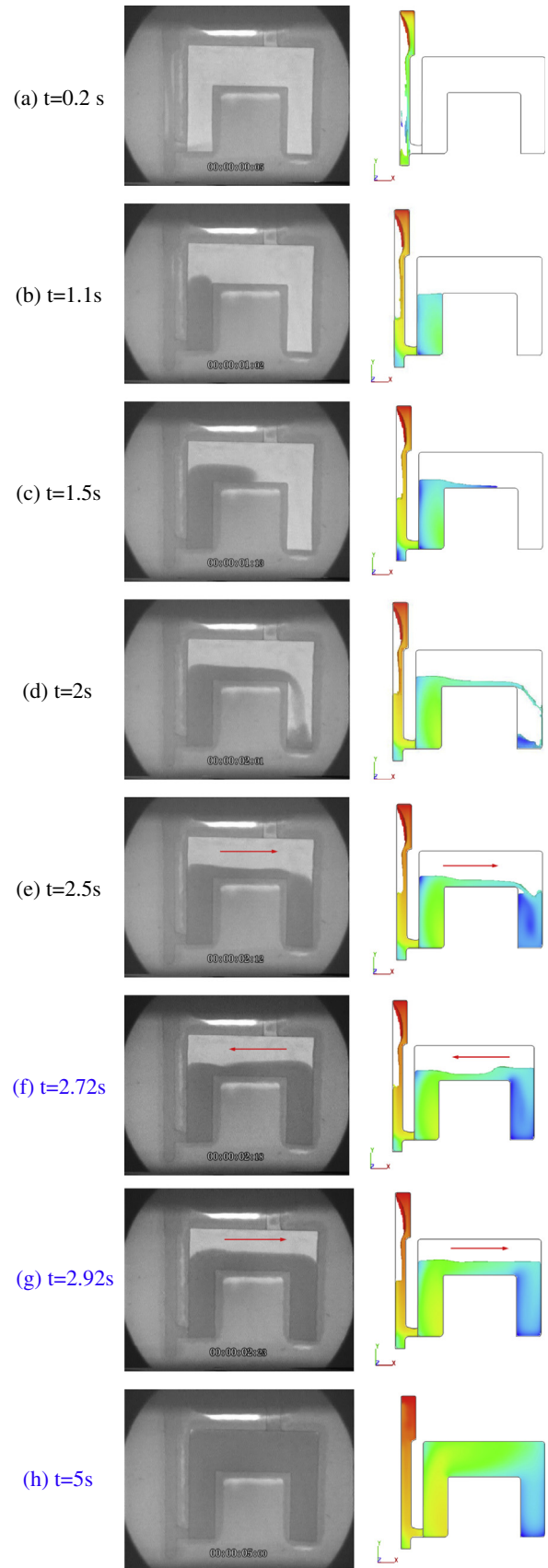


Fig. 5. Comparisons of flow behavior between simulation and experimental results at given time.

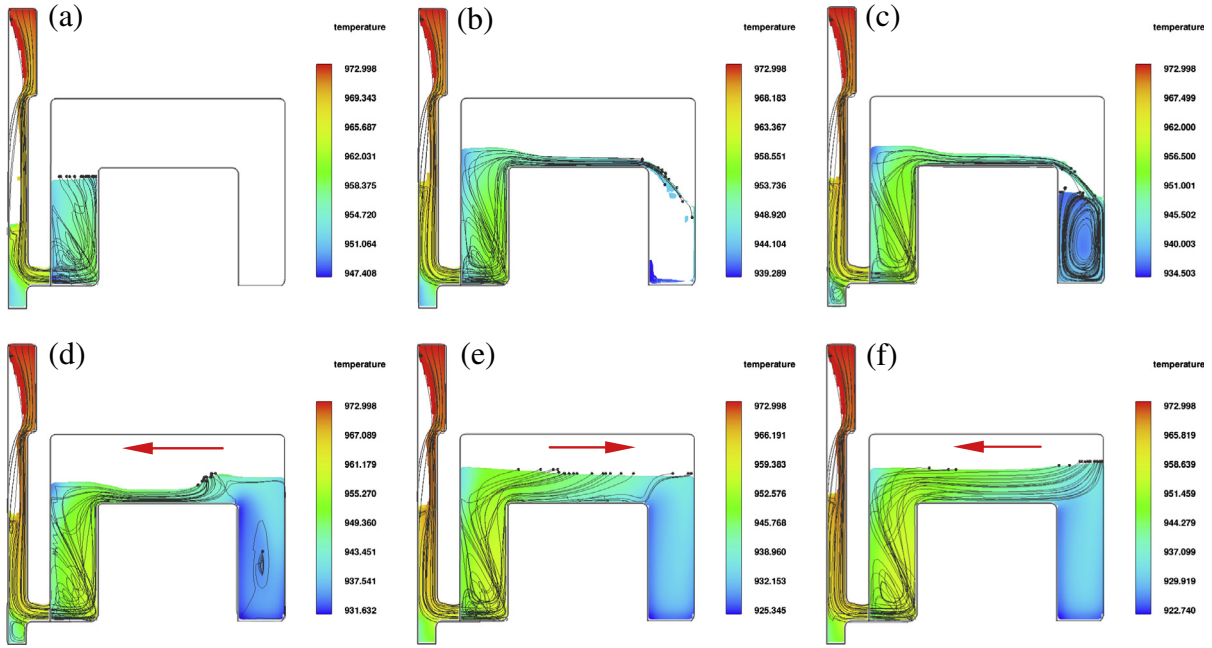


Fig. 6. Particle trajectories at different time during mold filling process: (a) 1.1 s, (b) 1.7 s, (c) 2.4 s, (d) 2.9 s, (e) 3.3 s, and (f) 3.5 s.

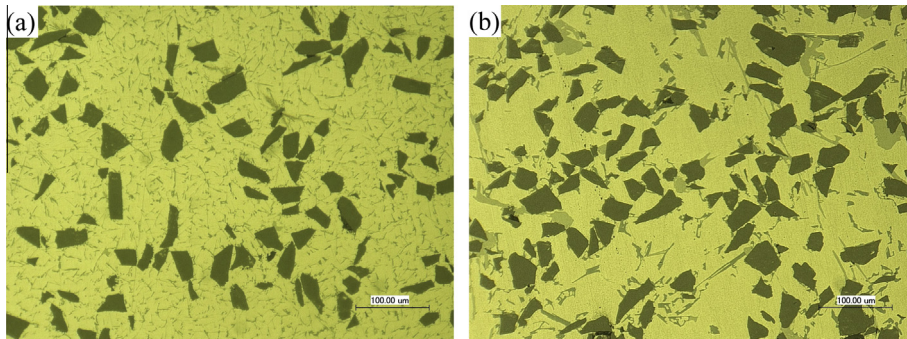


Fig. 7. Typical metallograph of the experimental castings: (a) after liquid stirring, and (b) after investment casting solidification.

with clear boundary distributed individually in the matrix (see Fig. 7a in the following section), indicating that the reaction products are rare and almost no clusters in the composite. Because there are very few interface reaction products and clusters in the composite, the impact of product and clusters on the flow behavior in the simulation were neglected.

Typical flow behavior of A356/SiCp composite during mold filling process is shown in Fig. 5. The results of simulation at selected stages of filling are compared with the results obtained from the real-time X-ray radiography experiment. The left-side and the right-side are the images of the real-time X-ray radiography and the predicted results of Flow-3D, respectively. In the simulation, top plane of the sprue is chosen as the boundary gate. Both the experimental and simulation results show that the stream reaches the bottom of the sprue at 0.2 s as shown in Fig. 5a, followed by passing through the ingate. Fig. 5b and c shows the status of fluid fills the anti-gravity and flow through the horizontal part, respectively. The filling statuses of the simulation results are similar to that of the experiment, but free surface shapes are different. The curvature of the free surface in the experiment is larger than that in the simulation. About at 2 s, the fluid begins to fill the gravity

part and eddy flow forms when the stream falls to the bottom of this part as shown in Fig. 5d. This feature continues as the ceramic shell is increasingly filled. The fluid fills the gravity part completely at 2.5 s (shown in Fig. 5e) and then fills the horizontal part (see Fig. 5f and g). Back flow occurs at this filling stage and the oscillations on the free surface are all reproduced both in simulation and real-time X-ray radiographic observed results. The surface wave reflects the right side of the horizontal part when the fluid has just filled the gravity part, and then travels to the left hitting the left wall and returning to the right. This sloshing free surface wave motion damps with the increase of filling ratio of the horizontal part. At 5 s, fluid substantially fills the whole cavity of the ceramic shell as shown in Fig. 5h.

In particle reinforced composites, the investigation of the particle flow can provide significant information for estimation the particle distribution. Due to the opacity of the fluid and resolution limit of the X-ray source, it is usually not practical to directly observe the particle flow in composite slurry. Simulation based on Lagrangian particle tracking is a powerful method for prediction the particle flow. Reilly et al. [27] used a similar method to model oxide film entrainment in casting systems and track the entrained

oxide films, and validation showed good quantitative correlation with experimental data. Fig. 6 shows the predicted results of selected particles flow trajectories at different times during mold filling. The arrows (Fig. 6d–f) indicate the surface wave flow direction after the back flow formed. Since it is impossible to track all the particles in the system, the motions of a few representative particles (25 particles) are tracked. The particle trajectories are irregular at anti-gravity part as shown in Fig. 6a, indicating that the particle flow pattern may be turbulent. As shown in Fig. 6b, the particles trajectories are almost parallel to each other, showing the laminar flow characteristic at the horizontal part. Fig. 6c presents the particle flow when the gravity part is filling. It can be seen that the particles set in motion by a large eddy tend to continue moving in the same helical trajectories and they are hard to leave the eddy. Fig. 6d–f display the particle trajectories during the slurry fills the horizontal part. At this stage, back flow occurs and the surface wave direction is moving from side to side. The particles flow directions are also change due to the back flow but the particle trajectories are still keep almost parallel. In addition, few particles continue flowing into the gravity part.

4.2. Particle distribution

Fig. 7 shows the optical microstructures after liquid stirring and investment casting solidification, respectively. It is seen that the particles with irregular shapes have good wettability with the matrix and almost all particle distribution is homogenous in the matrix. The average particle fractions at each region are listed in Table 2 and the representative metallographs in the central section are shown in Fig. 8. The average particle fractions of the whole

Table 2
Average particle fraction at each region (%).

Region	Central	Surface
R1	12.69	11.53
R2	10.99	10.18
R3	10.16	9.72
R4	10.83	10.95
R5	11.12	10.29
R6	10.73	9.17
R7	9.90	9.15
R8	10.04	9.20
Average	10.81	10.02

central and surface section are 10.81% and 10.02%, respectively. It is shown that there are more particles in the central section than in the section near the surface. This behavior may be caused by particle bouncing and migrating during mold filling, as well as by particle pushing during solidification.

During the mold filling process, a moving particle would bounce back if the normal velocity is non-zero when it collided with mold wall [29–31], which would influence the particle distribution. This phenomenon is demonstrated in the numerical simulation as shown in Fig. 9. Besides, particles tend to migrate to near-wall region under laminar flow condition while particles in the near-wall region will be pulled off by turbulent flow [32]. In this case, when the liquid metal passing through the ingate and entering the anti-gravity part, the predicted velocity from the simulation is about 0.92 m/s, and the equivalent diameter of the ingate is 8.9×10^{-3} m; when the fluid flowing through the horizontal part, the predicted velocity from the simulation is about 0.15 m/s, and the equivalent diameter is approximately 2.2×10^{-2} m. Based on the above data, the calculated Reynolds number at anti-gravity part and horizontal part are 5062 and 2040, respectively. According to the Reynolds number, the flow is turbulent at anti-gravity part and laminar at horizontal part. This may be the reason caused more particles distributed at surface than that at central cross section in R4 (see Table 2). During the stage of solidification, a thin layer of fine grain formed near the mold wall and particles could be pushed toward the center (shown in Fig. 10) by the growing primary α -Al grains due to the temperature gradients. As a result, more particles should be located in the center [1]. A similar tendency of particle distribution has been confirmed by Zhang et al. [12]. They investigated the particle distribution of Al-7% Si-10% B₄C die casting composite, and the quantitative analysis result showed that, in a cross-section of the cast part, more particles concentrate in the center and fewer particles were present in the die wall regions.

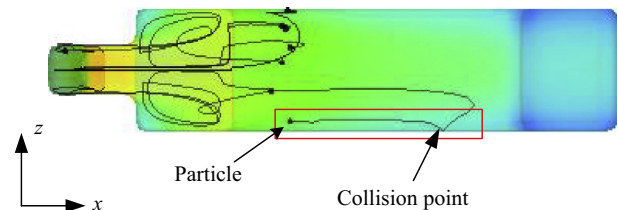


Fig. 9. Schematic of particle collide with mold wall.

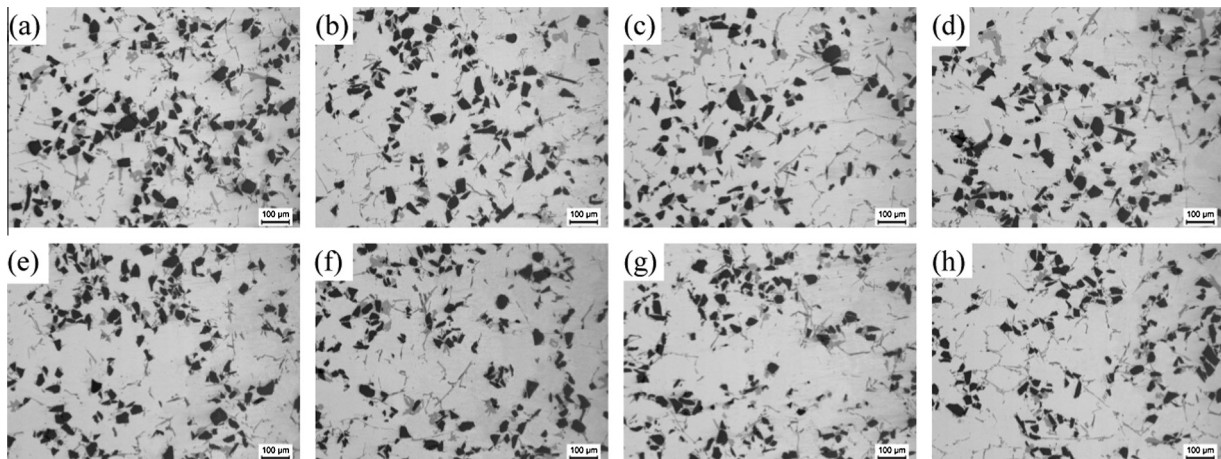


Fig. 8. Particle distribution in different regions at central section: (a)–(h) corresponds to regions R1–R8.

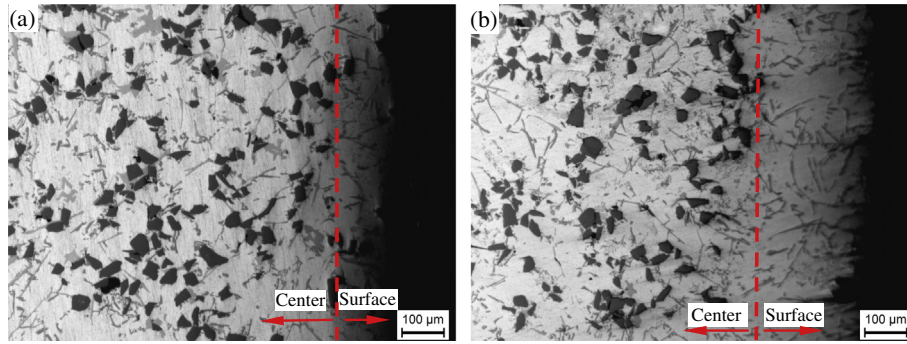


Fig. 10. Particle distribution near the surface: cross-section at (a) R2 and (b) R7.

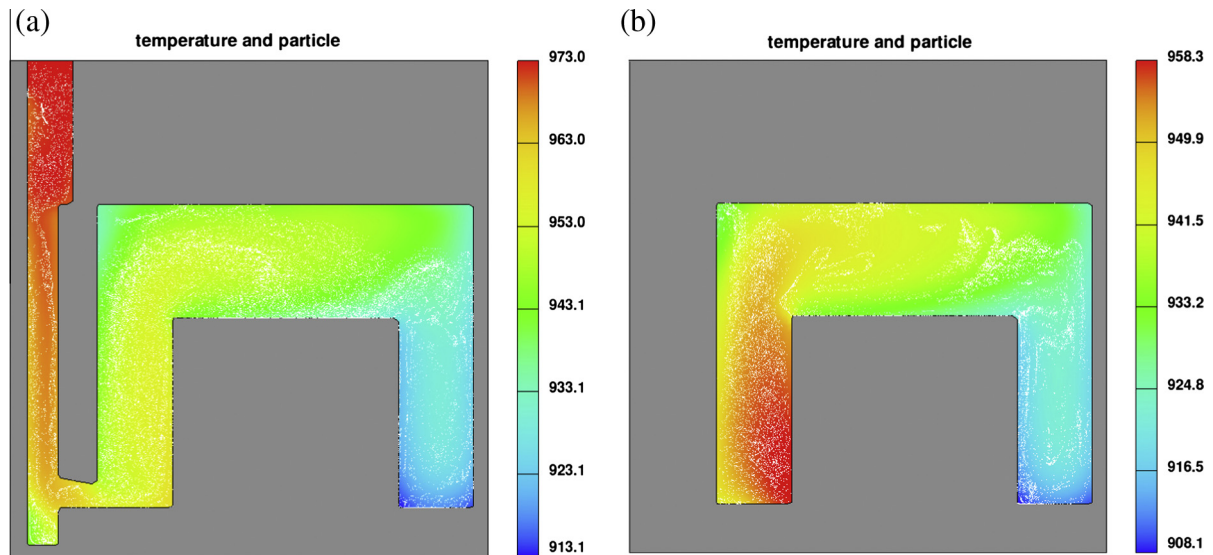


Fig. 11. Simulation results of particle distribution: (a) central and (b) surface section along the thickness direction.

Fig. 11 shows the simulation results of particle distribution at the central and surface section along the thickness direction, and the white points dispersed in the background indicate the SiC particles. It can be seen that the farther away from the ingate, the fewer particles both in central and surface sections. Similar results were presented by Mat and Aldas [33,34]. According to their works, the particle fractions decreased along the mold in suction casting. They considered that it was mainly caused by the particle trapping near the boundary wall in the lower section of the mold. In our viewpoints, flow behavior and particle trajectories also have significantly effect on particle distribution. In the present work, the casting near and far away from the ingate are anti-gravity and gravity part, respectively. At the anti-gravity part, the predicted results of particle trajectories show that the particle flow pattern is turbulent (see Fig. 6). And agitation induced by turbulence would increase the particle volumetric concentration [32], resulting in more particles disperse in this part [35]. At the gravity part, eddy flow occurs due to the inertia when the fluid falls to the bottom (as show in Figs. 5d and 6c). Particles are hardly to flow into or leave an eddy unless the eddy has broken up [36]. After the fluid had filled the gravity part, the back flow formed (see Fig. 5f) which will obstruct particles continuing flowing into the gravity part. In addition, the interaction between the particles and continue phase may also contribute to the particle distributed tendency. The relative velocity between particle and fluid is depended on the drag force to the

particle from the surrounding fluid (the second term in the right hand of Eq. (4)). According to Eq. (4), once the particle velocity is larger than that of the continue phase, the value of drag force term will becomes negative which will decrease the particle velocity, resulting in fewer particles in the filling front.

Fig. 12 shows the comparison of particle fractions at different regions between measured and predicted results. In order to compare conveniently, ξ (the ratio of the actual particle fraction to the largest fraction of each casting section) was used to represent the relative particle fraction. It is seen that particle fractions generally decreases with the increasing distance to the ingate. The simulation results agree satisfactorily with the experimental data except the gravity part. The particle fractions of simulation are less than that of experiment at this part, especially at R7 and R8 regions. This is perhaps caused by the back flow (see Fig. 5f). As mentioned before, back flow would obstruct the particles continuing flowing into these regions. Moreover, the particles move with the back flow and join the subsequent particles at horizontal part, resulting in more particles concentrate at R4 and R5 regions (see Table 2 and Fig. 12). The simulation result successfully predicts the back flow of fluid, but overestimates its influence on the particle flow. Almost none of particles are continuing flowing into R7 and R8 regions after the back flow occurs in the simulation as shown in Fig. 6d–f, while a few particles continuing flowing into those regions in the experiment.

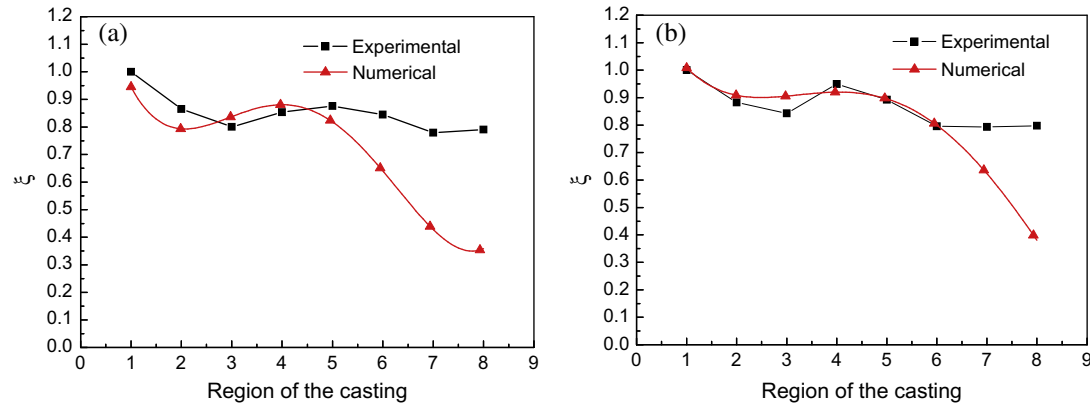


Fig. 12. Measured and predicted of particle fractions in the casting: (a) central and (b) surface section along the thickness direction.

5. Conclusions

Flow behavior and particle distribution in an inverted U-shape A356/SiCp composite Casting produced by conventional investment casting were experimentally and numerically investigated. The main conclusions can be summarized as follows:

The flow behavior of A356/SiCp composite and particle trajectories have significant effect on the particle distribution. Eddy flow is found at gravity part and after this part is full filled, the fluid fills the horizontal part and back flow occurs at this stage. The predicted results of particle trajectories show that particles are turbulence, laminar, and large eddy flow at anti-gravity, horizontal, and gravity part, respectively. Correspondingly, the particle fractions generally decrease with the increasing distance to the ingate which means more particles at anti-gravity part and fewer particles at gravity part. The simulation results agree well with the experimental data except the front part in which the particle fractions of the predicted results are fewer than those of the measured results.

The particle distribution along the thickness direction is also not uniform on a macro level. More particles concentrate in the central section, while fewer particles are present near the surface section.

Acknowledgements

This work was supported by the National 863 Project (Project No. 2013AA031201) and the National Natural Science Foundation of China (Project No. 50975093).

References

- [1] J. Hashim, L. Looney, M.S.J. Hashmi, Particle distribution in cast metal matrix composites – Part I, *J. Mater. Process. Technol.* 123 (2002) 251–257.
- [2] D.B. Miracle, Metal matrix composites—from science to technological significance, *Compos. Sci. Technol.* 65 (2005) 2526–2540.
- [3] B. Mondal, S. Kundu, A.K. Lohar, B.C. Pai, Net-shape manufacturing of intricate components of A356/SiCp composite through rapid-prototyping-integrated investment casting, *Mater. Sci. Eng. A* 498 (2008) 37–41.
- [4] S. Pattnaik, P.K. Jha, D.B. Karunakar, A review of rapid prototyping integrated investment casting processes, *Proc. Inst. Mech. Eng. L: J. Mater.* 228 (2014) 249–277.
- [5] B. Previtali, D. Pocchi, C. Taccardo, Application of traditional investment casting process to aluminium matrix composites, *Composites A* 39 (2008) 1606–1617.
- [6] P.N. Bindumadhavan, T.K. Chia, M. Chandrasekaran, H.K. Wah, L.N. Lam, O. Prabhakar, Effect of particle-porosity clusters on tribological behavior of cast aluminum alloy A356–SiCp metal matrix composites, *Mater. Sci. Eng. A* 171 (2001) 268–273.
- [7] V.A. Romanova, R.R. Balokhonov, S. Schmauder, The influence of the reinforcing particle shape and interface strength on the fracture behavior of a metal matrix composite, *Acta Mater.* 57 (2009) 97–107.
- [8] D.J. Lloyd, Particle reinforced aluminum and magnesium matrix composites, *Int. Mater. Rev.* 39 (1994) 1–23.
- [9] J. Hashim, L. Looney, M.S.J. Hashmi, Particle distribution in cast metal matrix composites – Part II, *J. Mater. Process. Technol.* 123 (2002) 258–263.
- [10] S.B. Prabu, L. Karunamoorthy, S. Kathiresan, B. Mohan, Influence of stirring speed and stirring time on distribution of particles in cast metal matrix composite, *J. Mater. Process. Technol.* 171 (2006) 268–273.
- [11] S. Naher, D. Brabazon, L. Looney, Computational and experimental analysis of particulate distribution during Al–SiC MMC fabrication, *Composites: Part A* 38 (2007) 719–729.
- [12] Z. Zhang, X.G. Chen, A. Charette, Particle distribution and interfacial reactions of Al–7%Si–10%B₄C die casting composite, *J. Mater. Sci.* 42 (2007) 7354–7362.
- [13] C.E. Brennen, *Fundamentals of Multiphase Flows*, Cambridge University Press, London, 2005.
- [14] T.J. Heindel, J.N. Gray, T.C. Jensen, An X-ray system for visualizing fluid flows, *Flow Meas. Instrum.* 19 (2008) 67–78.
- [15] A. Seeger, K. Affeld, L. Goubergrits, U. Kertzschner, E. Wellenhofer, X-ray-based assessment of the three-dimensional velocity of the liquid phase in a bobble column, *Exp. Fluids* 31 (2001) 193–201.
- [16] B. Sirrell, M. Holliday, J. Campbell, Benchmark testing the flow and solidification modeling of Al castings, *JOM-US* 48 (1996) 20–23.
- [17] D.Z. Li, J. Campbell, Y.Y. Li, Filling system for investment cast Ni-base turbine blades, *J. Mater. Process. Technol.* 148 (2004) 310–316.
- [18] S. Kashiwai, I. Ohnaka, A. Kimastuka, T. Kaneyoshi, T. Ohmichi, J. Zhu, Numerical simulation and X-ray direct observation of mould filling during vacuum suction casting, *Int. J. Cast. Met. Res.* 18 (2005) 144–148.
- [19] H.D. Zhao, I. Ohnaka, J.D. Zhu, Modeling of mold filling of Al gravity casting and validation with X-ray in-situ observation, *Appl. Math. Model.* 32 (2008) 185–194.
- [20] A. Ureña, E.E. Martínez, P. Rodrigo, L. Gil, Oxidation treatments for SiC particles used as reinforcement in aluminium matrix composites, *Compos. Sci. Technol.* 64 (2004) 1843–1854.
- [21] J. Rams, A. Ureña, M. Campo, Dual layer silica coatings of SiC particle reinforcements in aluminium matrix composites, *Surf. Coat. Technol.* 200 (2006) 4017–4026.
- [22] T. Fan, D. Zhang, G. Yang, T. Shibayanagi, M. Naka, T. Sakata, H. Mori, Chemical reaction of SiCp/Al composites during multiple remelting, *Composites: Part A* 34 (2003) 291–299.
- [23] D.S.B. Heidary, F. Akhlaghi, Theoretical and experimental study on settling of SiC particles in composite slurries of aluminum A356/SiC, *Acta Mater.* 59 (2011) 4556–4568.
- [24] J.F. Wendt, *Computational Fluid Dynamics*, Springer-Verlag, Berlin Heidelberg, New York, 2009.
- [25] M. Sommerfeld, Validation of a stochastic Lagrangian modeling approach for inter-particle collision in homogeneous isotropic turbulence, *Int. J. Multiphase Flow* 27 (2001) 1829–1858.
- [26] J. Braszczyński, A. Zyska, Analysis of the influence of ceramic particles on the solidification process of metal matrix composites, *Mater. Sci. Eng. A* 278 (2000) 195–203.
- [27] C. Reilly, N.R. Green, M.R. Jolly, J.-C. Gebelin, The modelling of oxide film entrapment in casting systems using computational modeling, *Appl. Math. Model.* 37 (2013) 8451–8466.
- [28] K.R. Ravi, R.M. Pillai, B.C. Pai, M. Chakraborty, Influence of interfacial reaction on the fluidity of A356 Al–SiCp composites—a theoretical approach, *Metall. Mater. Trans. A* 38 (2007) 2531–2539.
- [29] N.G. Deen, M.V.S. Annaland, M.A.V. Hoef, J.A.M. Kuipers, Review of discrete particle modeling of fluidized beds, *Chem. Eng. Sci.* 62 (2007) 28–44.
- [30] C.J. Meyer, D.A. Deglon, Particle collision modeling – a review, *Miner. Eng.* 24 (2011) 719–730.
- [31] K. Yokoi, Numerical method for interaction among multi-particle, fluid and arbitrary shape structure, *J. Sci. Comput.* 46 (2011) 166–181.
- [32] V. Loisel, M. Abbas, O. Masbarnat, E. Climent, The effect of neutrally buoyant finite-size particles on channel flows in the laminar–turbulent transition regime, *Phys. Fluids* 25 (2013) 1–18.

- [33] M.D. Mat, K. Aldas, Experimental and numerical investigation of effect of particle size on particle distribution in particulate metal matrix composites, *Appl. Math. Comput.* 177 (2006) 300–307.
- [34] K. Aldas, M.D. Mat, Experimental and theoretical analysis of particle distribution in particulate metal matrix composites, *J. Mater. Process. Technol.* 160 (2005) 289–295.
- [35] A. Tamburini, A. Cipollina, G. Micale, A. Brucato, M. Ciofalo, CFD simulations of dense solid–liquid suspensions in baffled stirred tanks: prediction of solid particle distribution, *Chem. Eng. J.* 223 (2013) 875–890.
- [36] A.S. Berrouk, D.E. Stock, D. Laurence, J.J. Riley, Heavy particle dispersion from a point source in turbulent pipe flow, *Int. J. Multiphase Flow* 34 (2008) 916–923.